EMBRY-RIDDLE
Aeronautical University™
SCHOLARLY COMMONS

Mechanical Engineering - Daytona Beach   College of Engineering

An Inverse POD-RBF Network Approach to Parameter Estimation in Mechanics

Craig A. Rogers
University of Central Florida

Alain Kassab
University of Central Florida

Eduardo Divo
Embry-Riddle Aeronautical University, Eduardo.divo@erau.edu

Ziemowit Ostrowski
Silesian University of Technology

Ryszard Bialecki
Silesian University of Technology

Follow this and additional works at: https://commons.erau.edu/db-mechanical-engineering

Part of the Mechanical Engineering Commons

An inverse POD-RBF network approach to parameter estimation in mechanics

Craig A. Rogers[1], Alain Kassab[1], Eduardo Divo[1,2], Ziemowit Ostrowski[3], and Ryszard Bialecki[3]

[1]*Department of Mechanical, Materials and Aerospace, University of Central Florida, Orlando, USA*
[2]*School of Engineering Technology, Daytona State College, Daytona Beach, USA*
[3]*Institute of Thermal Technology, Faculty of Power and Environmental Protection, Silesian University of Technology, Gliwice, Poland*

Abstract: An inverse approach is formulated using proper orthogonal decomposition (POD) integrated with a trained radial basis function (RBF) network to estimate various physical parameters of a specimen with little prior knowledge of the system. To generate the truncated POD-RBF network utilized in the inverse problem, a series of direct solutions based on FEM, BEM or exact analytical solutions are used to generate a data set of temperatures or deformations within the system or body, each produced for a unique set of physical parameters. The data set is then transformed via POD to generate an orthonormal basis to accurately solve for the desired material characteristics using the Levenberg-Marquardt (LM) algorithm to minimize the objective least squares functional. While the POD-RBF inverse approach outlined in this paper focuses primarily in application to conduction heat transfer, elasticity, and fracture mechanics, this technique is designed to be directly applicable to other realistic conditions and/or relevant industrial problems.
Keywords: Proper orthogonal decomposition, inverse problem, parameter estimation, heat conduction, elasticity, fracture mechanics.

1. Introduction

The concept of proper orthogonal decomposition (POD) began over a century ago as a statistical tool developed by Pearson [**1**]. Since that time, this method has been redeveloped under various names and in vastly different applications. Depending on how the input data is utilized POD is also similarly known as Karhunen-Loéve decomposition (KLD), principal component analysis (PCA) or singular value decomposition (SVD) [2-8]. Furthermore, this technique has been implemented in various applications from signal processing and control theory, human face recognition, data compression, fluid mechanics, parameter estimation and many others. However, to the knowledge of the authors POD has never been extended into the field of inverse problems in fracture mechanics and additionally has little evidence of its application to inverse problems in elasticity.

The integration of POD into inverse methods arose due to the demanding task of repeatedly solving forward problems while varying certain parameters in the process of seeking the solution of an ill-posed inverse problem. Inverse methods have been studied for decades, and different techniques have been proposed by many authors to retrieve the best approximate solution [9-12] often relying on the concepts of regularization; however, other methods such as model reduction that decrease the degrees of freedom in the problem and/or filtering excess error also benefit the inverse problem solution. The method of POD capitalizes on the correlation between the known direct problem and the sought-after solution [13-16]. The POD can be used to produce a low-order, but high quality, approximation of the solution field. More specifically POD is

often capable of capturing dominant components (called principal components) of the data with typically only a few modes. This is due to the ability of POD to offer the best basis for least-squares approximation defining a set of vectors using a rotated coordinate frame, where the angles of rotation are denoted as the POD basis [13,17,18]. Of course, the primary reason POD is a favorable in solving inverse problems, is that it provides many features of the desired methods for solving inverse problems, such as model reduction, error filtration and regularization.

Specifically in this paper, we develop a method of RBF-trained POD that can be interpreted as a numerical variation of parameters method for the forward problem and we apply this to three different inverse engineering problems. First, a basic two dimensional heat conduction problem is modeled to estimate a spatially dependent thermal conductivity. This problem will be used to illustrate that the POD can have a direct correlation to the analytical eigenfunctions governing the system. The next example deals with a linear elastic bar in tension in order to estimate the isotropic material coefficients within a steel sample. Finally, a compact tension specimen, relevant in fracture mechanics, is used to estimate the crack length of a sample under a constant Mode 1 loading [20,21].

2. Method

The first step in the implementation of POD is the creation of the *snapshot* which is the collection of N sampled values of $\mathbf{u}$ - the field under consideration. In heat conduction problems the vector $\boldsymbol{u}$ stores the discrete temperature field while in elasticity the snapshot is a sampled deformation field. Next, a collection of M snapshots denoted as $\mathbf{u}^j$ (for $j = 1, 2 \ldots M$) are generated by altering the parameter(s) upon which the field depends on. In the current scope, the altered parameters refer to the parameters describing the spatial distribution of the conductivity, Young modulus and Poisson ratio as well as the crack length. Generally the altered parameters can be any selection of material properties and/or boundary conditions. Each $\mathbf{u}^j$ is then stored inside rectangular $N \times M$ matrix $\mathbf{U}$ denoted as the snapshot matrix. The snapshot field may be created by numerical modeling of the system, say FEM or BEM, sampling an analytical solution or from actual empirical data. The goal of POD is to establish a set of orthonormal vectors $\boldsymbol{\Phi}^j$ (for $j = 1, 2 \ldots M$) resembling the snapshot matrix $\mathbf{U}$ in an optimal way. The matrix $\boldsymbol{\Phi}$ is commonly referred to as the POD *basis* and can be seen in (1)(1) .

$$\boldsymbol{\Phi} = \mathbf{U} \cdot \mathbf{V}$$

1()

$\mathbf{V}$ represents the eigenvectors of the covariance matrix $\mathbf{C}$ and can easily be derived using the nontrivial solution of the general eigenvalue problem denoted in (2)(2).

$$\mathbf{C} \cdot \mathbf{V} = \quad \cdot$$

2()

$\boldsymbol{\Lambda}$ represents a diagonal matrix that stores the eigenvalues λ of the covariance matrix $\mathbf{C}$, which is defined in (3)(3).

$$\mathbf{C} = \mathbf{U}^{\mathrm{T}} \cdot \mathbf{U}$$

3()

It may also serve to note that $\mathbf{C}$ is symmetric and positive definite and λ is always real and positive. Typically λ is sorted in a descending order and can often be attributed to the energy of the POD mode (base vector). This energy decreases rapidly with the increasing mode number. Since higher modes hold little energy (or data) of the system they can be discarded without influencing the accuracy of representation (1). This is known as the truncation of the POD basis and is accomplished by deciding which fraction of the energy of the system can be neglected in later calculations. The resulting POD basis $\tilde{\mathbf{\Phi}}$, referred to as the *truncated* POD basis consists of $K < M$ vectors and is shown in (4)(4).

$$\tilde{\mathbf{\Phi}} = \mathbf{U} \cdot \tilde{\mathbf{V}}$$

4()

This also corresponds to the truncation of the eigenvector matrix, denoted as $\tilde{\mathbf{V}}$, which stores the first K^{th} eigenvectors of $\mathbf{C}$. The truncated POD basis (4)(4) is also known to be orthogonal $\mathbf{\Phi}^{\mathrm{T}} \cdot \mathbf{\Phi} = \mathbf{I}$ and presents optimal approximation properties. Once $\tilde{\mathbf{\Phi}}$ is known, the snapshot matrix $\mathbf{U}$ can be regenerated and approximated as (5)(5).

$$\mathbf{U} = \mathbf{A}^{J} \cdot$$

5()

$\mathbf{A}$ stands for the amplitudes associated with $\mathbf{u}^j$. Now referring to the orthogonality of $\tilde{\mathbf{\Phi}}$, the amplitudes can be determined from (6)(6).

$$\mathbf{A} = \tilde{\mathbf{U}}^{\mathrm{T}} \cdot$$

6()

At this time, data may begin to be extrapolated for information on the current problem. To do this, consider a vector $\mathbf{p}$ which stores the parameters on which the solution depends. The transient derivation is not further described in this paper, for more information refer to [4,5].

Next, the amplitudes $\mathbf{A}$ are defined as a nonlinear function of the parameter vector $\mathbf{p}$. The unknown constant coefficients of the current combination are gathered in a matrix $\mathbf{B}$, shown as (7)(7).

$$\mathbf{A} = \mathbf{B} \cdot \mathbf{F}$$

7()

$\mathbf{F}$ is defined as the matrix of interpolation functions, where the set of interpolation functions $f_i(\mathbf{p})$ can be chosen arbitrarily. However, some choices of interpolation functions may lead to an ill-conditioned system of equations for the coefficient matrix $\mathbf{B}$. In this paper, radial basis functions (RBF's) have been used as the interpolating function of choice due to their nice approximation and smoothing properties. Here the Hardy inverse multi-quadric radial basis function [22,23] has been employed.

$$f_i(\mathbf{p}) = f_i(\|\mathbf{p} - \mathbf{p}^i\|) = \frac{1}{\sqrt{\|\mathbf{p} - \mathbf{p}^i\|^2 + c^2}}$$

8()

Where c is defined as the RBF smoothing factor and $\mathbf{p}^i$ corresponds to the same parameter $\mathbf{p}$ used to generate $\mathbf{u}^i$ (for $i = 1, 2 \dots M$). The smoothing parameter, c, is chosen to push the conditioning number of the RBF interpolation matrix $\mathbf{F}$, defined below, as high as numerically possible in order to obtain the highest order interpolation from the RBF [24-26]. It should be seen that the argument of the ith RBF is the distance $|\mathbf{p} - \mathbf{p}^i|$ between its current parameter $\mathbf{p}$ and the reference parameter $\mathbf{p}^i$.

To use (7)(7), the matrix of coefficients $\mathbf{B}$ needs to be evaluated. This can be done by simple inversion

$$\mathbf{B} = \mathbf{A} \cdot \mathbf{F}^{-1}$$

9()

As stated previously, $\mathbf{F}$ is the matrix of interpolation functions defined as set of M identical vectors $\mathbf{f}(\mathbf{p})$ defined as $\{\mathbf{f}\}_j = f_j\left(\left|\mathbf{p} - \mathbf{p}^j\right|\right)$. Requiring that (9) is exact for all vectors used to generate the snapshots, leads to a definition of the $\mathbf{F}$ matrix.

$$\mathbf{F} = \begin{bmatrix} f_1(|\mathbf{p}^1 - \mathbf{p}^1|) & \mathsf{L} & f_1(|\mathbf{p}^j - \mathbf{p}^1|) & \mathsf{L} & f_1(|\mathbf{p}^M - \mathbf{p}^1|) \\ \mathsf{M} & & \mathsf{M} & & \mathsf{M} \\ f_i(|\mathbf{p}^1 - \mathbf{p}^i|) & \mathsf{L} & f_i(|\mathbf{p}^j - \mathbf{p}^i|) & \mathsf{L} & f_i(|\mathbf{p}^M - \mathbf{p}^i|) \\ \mathsf{M} & & \mathsf{M} & & \mathsf{M} \\ f_M(|\mathbf{p}^1 - \mathbf{p}^M|) & \mathsf{L} & f_M(|\mathbf{p}^j - \mathbf{p}^M|) & \mathsf{L} & f_M(|\mathbf{p}^M - \mathbf{p}^M|) \end{bmatrix}$$

10()

With $\mathbf{p}^i$ and $\mathbf{p}^j$ vectors of parameters used to generate i^{th} or j^{th} snapshot respectively.

At this point it should be stressed that the matrix of amplitudes $\mathbf{A}$ and the matrix of coefficients $\mathbf{B}$ are known using the above relations. Now equating (6)(6) and (7)(7) yields the following.

$$\boldsymbol{\Phi}^T \cdot \mathbf{U} = \mathbf{B} \cdot \mathbf{F}$$

11()

Using the orthogonality of $\boldsymbol{\Phi}$, it can easily be seen that the snapshot matrix $\mathbf{U}$ can be approximated as (12)(12).

$$\mathbf{U}(\mathbf{p}) \approx \boldsymbol{\Phi} \cdot \mathbf{B} \cdot \mathbf{f}'(\mathbf{p}) \cdot (\,)$$

12()

Such that after the coefficient matrix $\mathbf{B}$ is evaluated, a low dimensional model of (5)(5), now defined as (12)(12), can be set in vector form as (13)(13).

$$\mathbf{u}(\mathbf{p}) \approx \boldsymbol{\Phi} \cdot \mathbf{B} \cdot \mathbf{f}'(\mathbf{p}) \cdot (\,)$$

13()

This model will now be referred to as the *trained* POD-RBF network and is completely capable of reproducing the unknown field that corresponds to any arbitrary set of parameters $\mathbf{p}$. This

can be thought of as a numerical eingenfunction expansion of the solution reminiscent of the variation of parameters (or integral transform) method for the analytical solution of partial differential equations. It must be noted, that extrapolation outside the range of **p** used to generate the initial snapshots **u**^{i} can lead to poor accuracy of the model.

Finally, the trained POD-RBF network in (13)(13) is used to retrieve the values of the unknown parameter vector **p**. This is done in a least squares sense by taking the sum of the squares of the data obtained from (13)(13) and subtracting it from the actual experimental data *y*. To avoid additional interpolation, the sampling points of the field should coincide with the sensor locations. Finally, a least-squares functional is augmented with the aid of a regularization term

$$\Psi(\mathbf{p}) = \sum_{i=1}^{N} \left(u(\mathbf{p}^i) - y_i\right)^2 + \alpha \sum_{i=1}^{N} \left(u_i(\mathbf{p}) - \bar{y}\right)^2$$

$$14()$$

and minimized with respect to the variable **p** using the Levenberg-Marquardt algorithm. First order regularization is performed with respect to the mean of the data $\bar{y}$, a variation of the approach in [27,28] where the regularization is carried out with respect to deviation from the running least squares fit of the data. The regularization parameter is obtained by means of the L-curve method of Hansen [29,30].

3. Results

Three numerical examples are outlined which cover the estimation of various material characteristics or properties within each sample. The first example illustrates the estimation of a spatially dependent thermal conductivity within a two dimensional heat conduction domain. In the next example, the isotropic material constants are found using a three dimensional bar in tension modeled using FEM. Lastly, a linear elastic fracture mechanics (LEFM) example is used to accurately estimate the crack length of a compact tension specimen under a constant Mode 1 loading. We do not use results from physical measurements, instead, virtual measurements are generated by solving a reference forward problem. The obtained values at selected points are then laden by a randomly generated error and used as simulated measurements in the inverse algorithm. In the next step, a sequence of forward problems is solved using selected values of the parameters to be retrieved to produce the snapshots that are processed using the POD-RBF technique. In the last step the least square fit of POD-RBF and virtual measurements is carried out producing the required material parameters. In order to avoid the so-called inverse crime [31], a different mesh and/or modified elements are used when solving the reference forward problem and generating the snapshots.

3.1. Heat Conduction – Square Region

In the first example, the POD-RBF network is utilized to approximate the temperature distribution at points within a square block shown in Figure 1Figure 1Figure 1, as well as estimate the spatially dependent thermal conductivity.

k´ `

T(0,y)

X=0   X=L
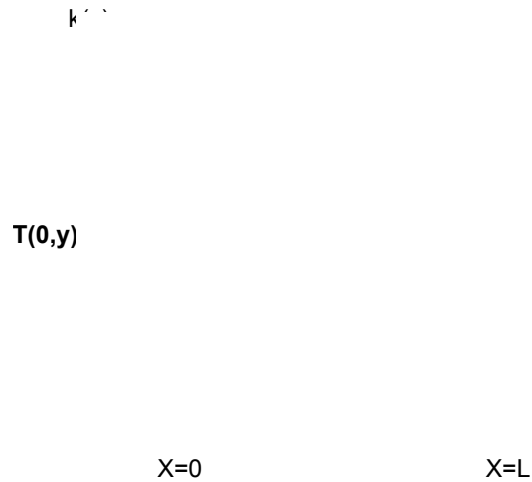
Figure 1 - Illustration of square domain for heat conduction case with nodal location numbering.

The thermal conductivity is assumed to be a linear function of the x (horizontal) direction

$$k\left(x\right)=a+bx$$

15()

where $k(x)$ denotes the thermal conductivity at some point x within the domain. Hardy inverse RBF interpolation equation can be seen as

$$f_i\left(k\left(a,b\right)\right)=\frac{1}{\sqrt{k\left(a,b\right)^2+r^2}}$$

16()

where

$$k\left(a,b\right)=\left[a+bx\right]-p^i$$

17()

which is then used to approximate the temperature distributions **u** within the body.

$$\Phi(a,b) \approx \hat{} \cdot \cdot \left(k\left(a,b\right)\right)$$

18()

The temperature distributions (or the snapshot vector **u**) are then used to estimate the constants of the spatially dependent thermal conductivity shown in (15)(15), using the least squares objective function utilized by LM.

In this example, **p** collects the thermal conductivity constants to be determined

$$\mathbf{p}=\begin{pmatrix}a\\b\end{pmatrix}$$

19()

For the initial validation case, the thermal conductivity constants are set as $a = 1.234$ and $b = 3.456$. It can readily be checked that the direct heat conduction problem has the following exact solution

$$T(x,y) = \frac{C}{b}\ln(a+bx) + Dy + E$$

20()

where the values of the arbitrary constants C, D and E were chosen as $C=100$, $D=10$ and $E = 0$. The snapshot matrix $\mathbf{U}$ is then set up using 16 equally spaced nodes N throughout the square region. A total of 100 snapshots M were created using various values of a and b arising in the definition of the thermal conductivity field $k(x)$,

The first five eigenvalues of the covariance matrix associated with subsequent POD modes are shown in Table 1Table 1Table 1. Only five POD modes were used in further analysis.

Table 1 - Table of truncated eigenvalues of square region heat conduction case

	λ_1	λ_2	λ_3	λ_4	λ_5
λ	9.61E+06	1.72E+04	1.35E+03	2.39E+01	2.60E-02

It is important to note that at this point that the standard inverse analysis (without regularization) may produce inaccurate and unstable results. Proper selection of the regularization parameter α cures this situation. The question of an optimal selection of the regularization constant is outside the context of this paper and will not be discussed further, suffice it to say that the L-curve method of Hansen was utilized and for more information regarding the selection of the regularization constant refer to [18]. Once the regularization parameter is selected, the POD-RBF inverse approach can be fully implemented to estimate the temperature distribution and thermal conductivity constants within the system.

The POD-RBF estimation of the temperature distribution and its corresponding error are shown in Figure 2Figure 2Figure 2. More importantly, the approximation of the thermal conductivity constants and its distribution through the domain is shown in Figure 3Figure 3Figure 3 and Table 2Table 2Table 2. The results were produced without adding random error to the virtual measurements.
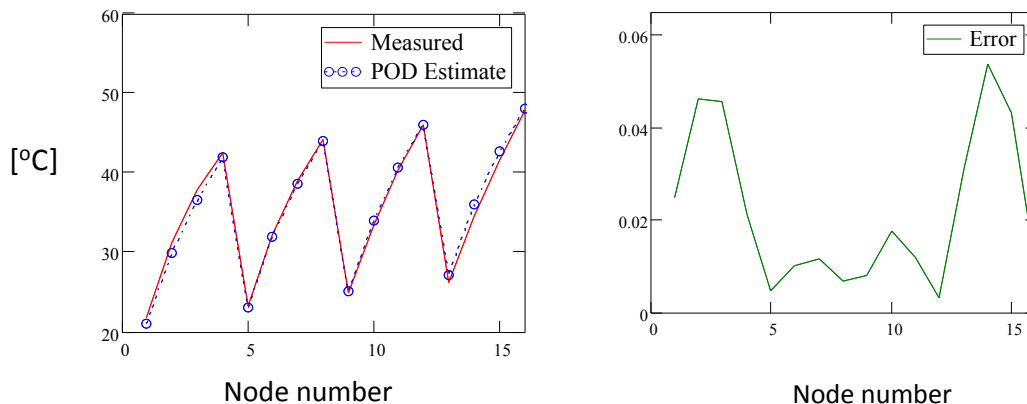
Figure 2 - Comparison of exact solution against POD estimation of temperature distribution for square region as well as percent error.
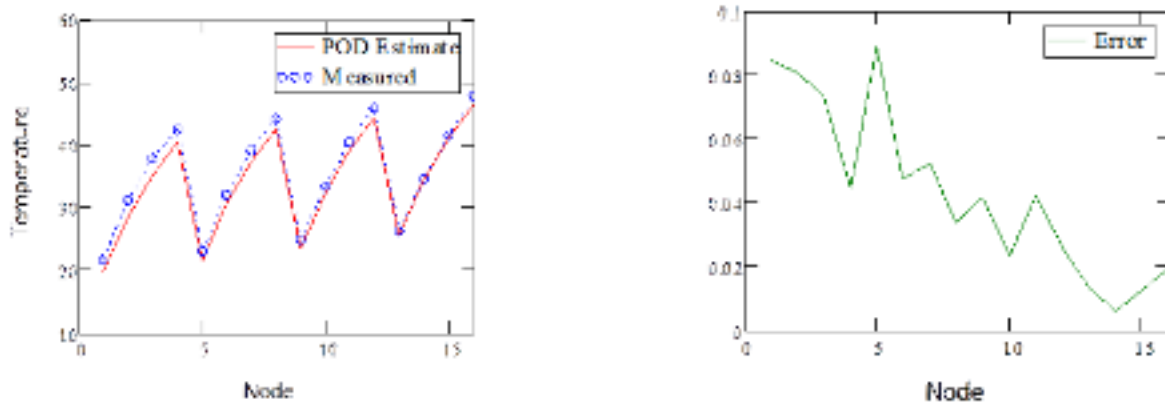
Figure 3 - Comparison of POD-RBF estimate of thermal conductivity against measured data for square region

Table 2 – Table of POD-RBF estimated spatially dependent thermal conductivity constants and their errors

	Actual	Estimate	Error
a	1.234	1.169	5.27%
b	3.456	3.668	6.13%

It can be seen that the error produced in the POD-RBF approximation of the temperature field is never larger the 6% for this example. Accordingly, the POD-RBF inverse method produces an accurate approximation of the thermal conductivity parameters. In an experimental sense, instrumentation error would create noise in the data reading which may skew the POD-RBF approximation.

In order to accommodate this, a random normal distribution error is added to the analytical solution to represent instrumentation noise from data collection. Noise at an amplitude of $\pm 0.5^{\circ}$ is added to the solution and the POD-RBF inverse approach is then reapplied to the system. The corresponding results are shown in Figure 4Figure 4Figure 4, Figure 5Figure 5Figure 5 and Table 3Table 3Table 3.

Figure 4 - Comparison of measured noisy (± 0.5º) data against POD estimation of temperature distribution for square region.

Figure 5 - Comparison of POD-RBF estimate of thermal conductivity against measured noisy (± 0.5º) data for square region

Table 3 – Table of spatially dependent thermal conductivity constants and their corresponding errors with noise added to represent empirical data collection.

	Actual	Estimate	Error
a	1.234	1.157	6.24%
b	3.456	3.645	5.47%

As in the previous case, the accuracy of the procedure is good showing that the POD-RBF solver is not sensitive to the random measurement error.

The solution of the heat conduction problem in finite domains produced by separation of variables has a form of an infinite series of eigenfunctions. Thus, the eignefunctions play an important role in the theory of Fourier series. An important fact that should be further noted is similarity of the POD basis vectors to the analytical eigenfunctions of the problem.

$$eig(x, y) = \sin\left(\frac{n\pi x}{L}\right)\cos\left(\frac{m\pi y}{L}\right)$$

21()

Where *x* and *y* are physical locations throughout the domain and *n = 1, 2, 3…* and *m = 0, 1, 2…* Applying the analytical eigenfunction to the current square domain yields the following in Figure 6Figure 6Figure 6. It should be noted that eigenfunctions are typically two dimensional plots when displayed. However, to show direct comparison of the analytical eigenfunctions to the POD basis vectors; these vectors are plotted point-wise at each node for easier visualization and direct comparison.

n = 2; m = 0
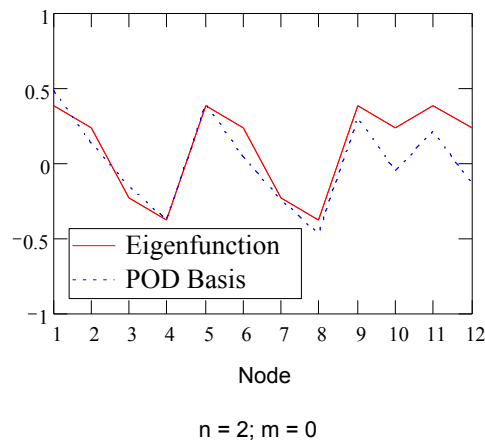
Figure 6 - Comparison of selected analytical eigenfunctions to POD basis vectors with the corresponding indices shown below each figure.

Accordingly, this realization helps to show that the POD transformation has some physical interpretation and is closely associated with the Fourier expansion of the solution of the direct problem. In a more complex sense, the POD basis vectors may be used to represent the eigenfunctions, when an analytical solution is hard and/or laborious to derive effectively.

3.2. Heat Conduction – L Region

Now a variation of the previous heat conduction example will be studied using a more complex "L" shaped domain as illustrated in Figure 7Figure 7Figure 7.
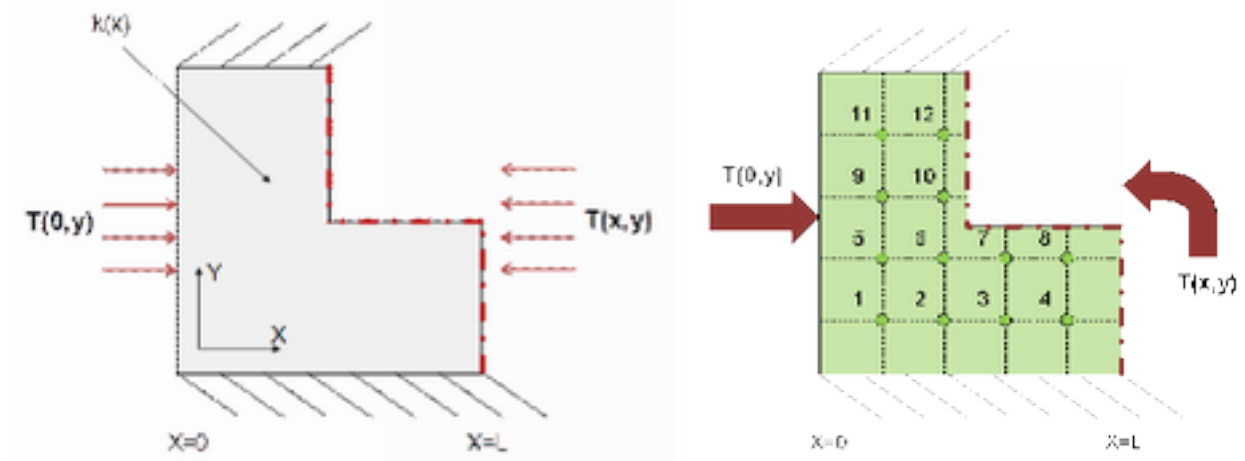
**Figure 7 - Illustration of L shaped region for heat conduction case.**

Since the only changes to the previous heat conduction example will be to the domain, the same POD-RBF derivations can therefore be applied from above, except that the exact solution was now solved using highly accurate in-house BEM software. Accordingly, the main objective of this subsequent section is to study how the change in domain will effect the POD-RBF approximation, if any.

The temperature field is now set up using 12 nodes spaced throughout the domain using 100 snapshots to create the snapshot matrix **U**. Likewise, the first five eigenvalues of the covariance matrix associated with subsequent POD modes are shown in Table 4Table 4Table 4. These modes were truncated after the fifth term of a possible 100 for comparison to the previous example.

Table 4 - Table of truncated eigenvalues of L region heat conduction case

	λ_1	λ_2	λ_3	λ_4	λ_5
λ	6.56E+06	9.62E+04	1.03E+03	1.82E+01	1.50E-02

For initial verification, the first case will incorporate a no noise solution with the results outlined in Figure 8Figure 8Figure 8 - Figure 9Figure 9Figure 9.
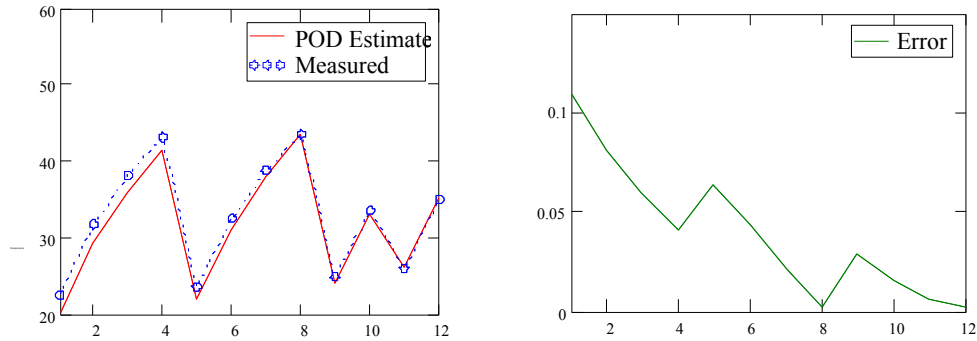
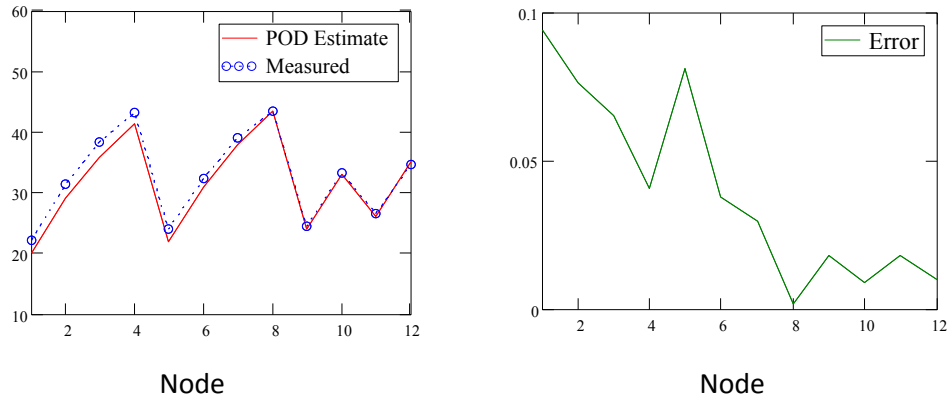**Figure 8 - Comparison of measured data against POD estimation of temperature distribution for L region.**

Figure 9 - Comparison of POD-RBF estimate of thermal conductivity against measured data for L region

Again the temperature distribution and thermal conductivity are estimated accurately using the POD-RBF technique, despite the shape of the domain. With a maximum error slightly above 10%, the POD technique is still extremely accurate considering only 5 POD modes were used to estimate the system. The new spatially dependent thermal conductivity constants for the renovated ("L") region can be observed in Table 5Table 5Table 5 below.

Table 5 - Comparison of Measured and POD-RBF estimation of thermal conductivity of L region

	Actual	Estimate	Error
a	1.234	1.182	4.21%
b	3.456	3.486	0.87%

Of course instrumentation error would create noise in the data reading which may skew the POD-RBF approximation. In order to accommodate instrumentation errors, a random normal distribution error is added to the solution to represent noise during data collection. Noise at amplitudes of ± 0.5º is added to the solution to act as empirical data and the POD-RBF inverse approach is reapplied to the system. The corresponding results are shown below in Figure 10Figure 10Figure 10 - Figure 11Figure 11Figure 11.

Figure 10 - Comparison of measured noisy (± 0.5º) data against POD estimation of temperature distribution for L region.

Figure 11 - Comparison of POD-RBF estimate of thermal conductivity against measured noisy (± 0.5º) data for L region

Despite the noise present within the data, the POD-RBF network is still able to estimate the temperature field and thermal conductivity constants quickly and efficiently. The estimated thermal conductivity constants from the corresponding noisy data are shown in Table 6Table 6Table 6.

Table 6 - Comparison of Measured and POD-RBF estimation of thermal conductivity of L region

	Actual	Estimate	Error
a	1.234	1.177	4.62%
b	3.456	3.504	1.39%

In comparison to the previous heat transfer section, the POD-RBF inverse method still produces highly accurate results despite the shape of the domain being used. This is a great find as it can allow the POD-RBF technique to take on more complicated domains and still maintain ideal approximation capabilities.

Furthermore, the POD basis vectors can be shown to once again have a direct correlation to the analytical eigenfunctions derived from Fourier analysis. However, the eigenfunctions for the L

shaped domain cannot be derived, rather, the POD basis for the L-shaped domain are compared to the analytical eigenfuctions of the embedding square region domain of the previous problem. This comparison is provided in Figure 12 which shows that this is indeed the case.
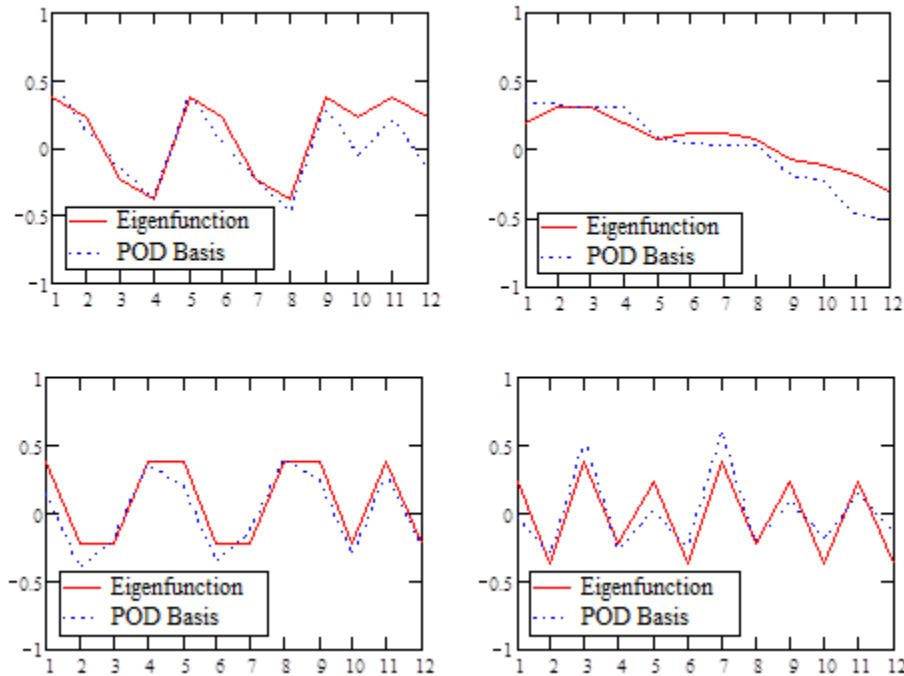

Figure 12 - Comparison of analytical eigenfunctions to POD basis vectors in L shaped domain.

3.3. Elasticity

This next application uses the POD-RBF inverse technique to estimate the isotropic material parameters of a three dimensional bar in tension. The isotropic constants are denoted as for the modul. Using basic relations from linear elasticity, the three material parameters are related using

$$E = 2G(1+\nu)$$

22()

This relation will be used to establish the initial parameter matrix which will be referred to during RBF extrapolation for the inverse approximation. The deflections are calculated using FEM and are set up to be extracted at several simulated strain gage locations on the beam. In order to avoid the irrefutable inverse crime, a new mesh is generated in order to obtain the measured or experimental deflections.
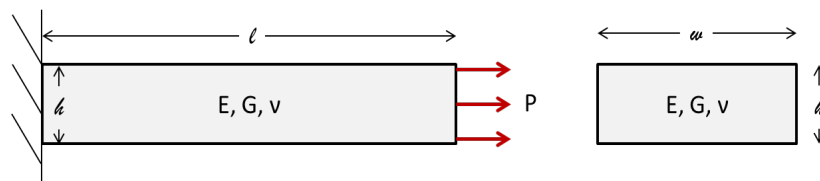

Figure 13 - 3D bar in tension.

The snapshot matrix **U** was created using only six nodes on three surfaces of the beam, taking a total 36 snapshots at various elastic parameters **p**. POD was then performed to produce the eigenvalues shown in Table 7Table 7Table 7 which were truncated after the 6th term of a possible 36.

Table 7 - Table of truncated eigenvalues for 3D elasticity case

	λ_1	λ_2	λ_3	λ_4	λ_5	λ_6
λ	5.12E+06	8.73E+01	4.78E-01	4.25E-01	2.93E-01	2.56E-01

.
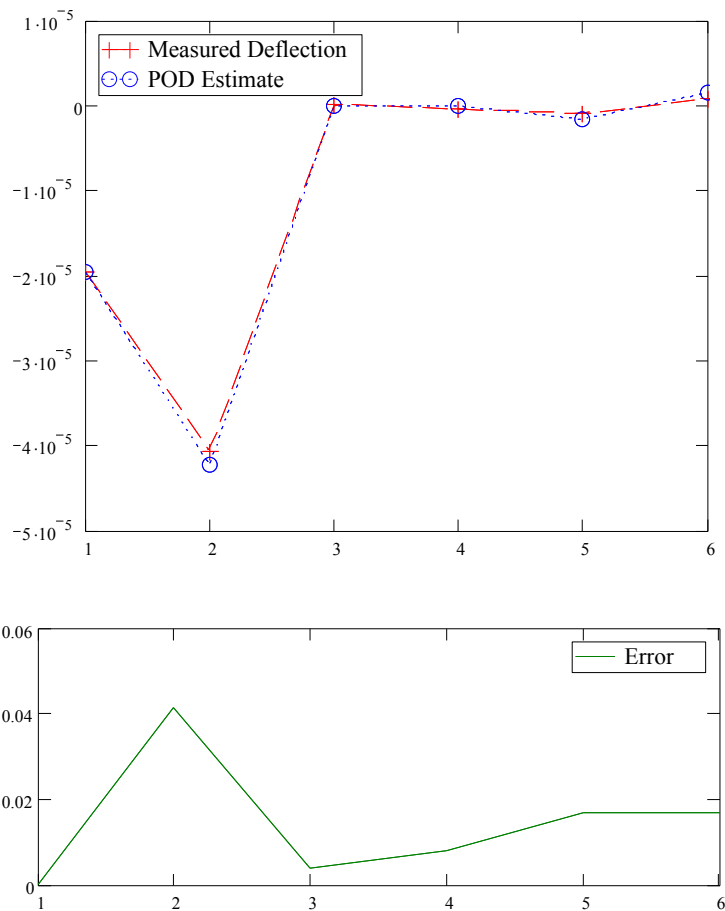
Figure 14 - Comparison of FEM solution against the POD-RBF approximation of the deflection in for an elastic bean under tension and the accompanying % nodal error.
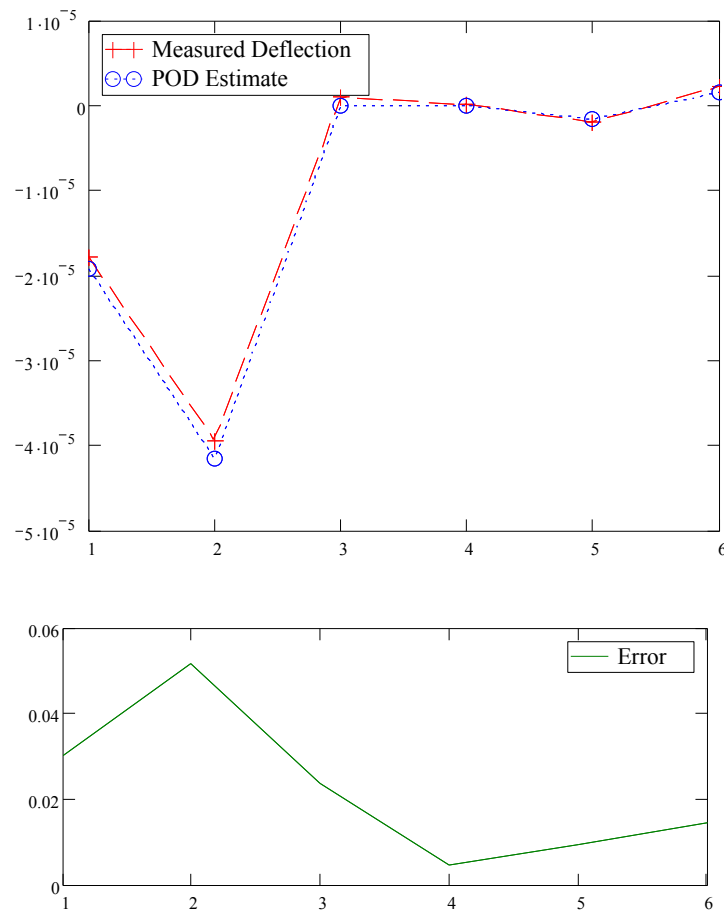
Table 8 - Comparison of Actual and POD-RBF estimation of material parameters for 3D elasticity

	Actual	Estimate	Error
Modulus of Elasticity, E	206.85 GPa	209.99 GPa	1.52%
Shear Modulus, G	80.8 GPa	82.43 GPa	2.02%
Poisson's ratio, ν	0.28	0.274	2.14%

This first example is used only as a verification of the POD-RBF inverse technique in elasticity. That is because this example does not incorporate any so-called "experimental noise" to the FEM solution other than the addition of standard interpolation or numerical error generated from the presence of a new mesh.

In order to reproduce experimental data collection, noise is added to the FEM solution. The amplitude of noise was taken as ± 10% of the measured FEM solution. Reapplying the POD-RBF inverse technique then produced the following results shown in Figure 15Figure 1516Figure 16 and Table 9Table 9Table 9.

Figure 151516 - Comparison of the POD-RBF approximation against the noisy data (± 10 %) in each Cartesian direction for 3D elasticity

Table 9 - Comparison of Actual and POD-RBF estimation of material parameters for noisy data (± 10 %) measurements in 3D elasticity

|	Actual	Estimate	Error
Modulus of Elasticity, E	206.85 GPa	209.79 GPa	1.42%
Shear Modulus, G	80.8 GPa	81.64 GPa	1.04%
Poisson's ratio, ν	0.28	0.285	1.79%

For the error-laden problem at hand, the POD-RBF inverse technique was still able to reproduce accurate estimations of the material parameters even in the presence of larger amounts of noise. In fact POD is extremely robust to the deleterious effects of measurement noise [13-16]. This is essentially due to the regularization within POD which tries to achieve the same mean value within the POD approximated data and the measured data.

As denoted in the previous section, the POD basis vectors have the ability to retain some physical aspects of the governing system. In terms of heat transfer, these aspects were the analytical eigenfunctions. In reference [6], the authors show that the POD basis vectors can be physically correlated in elasticity with the eigenmodes or mode shapes of the domain. This is the practical reasoning behind other names often used to refer to POD such as Proper Orthogonal Modes or Empirical Eigenfunctions.

3.4. Fracture Mechanics

The final application is in fracture mechanic where a compact tension C(T) specimen is modeled using FEM software and the above POD-RBF inverse approach is applied to determine the unknown crack length for a standard C(T) specimen. The C(T) specimen was modeled following ASTM E399 standards for plain strain fracture toughness and can be seen in Figure 16Figure 16Figure 18.
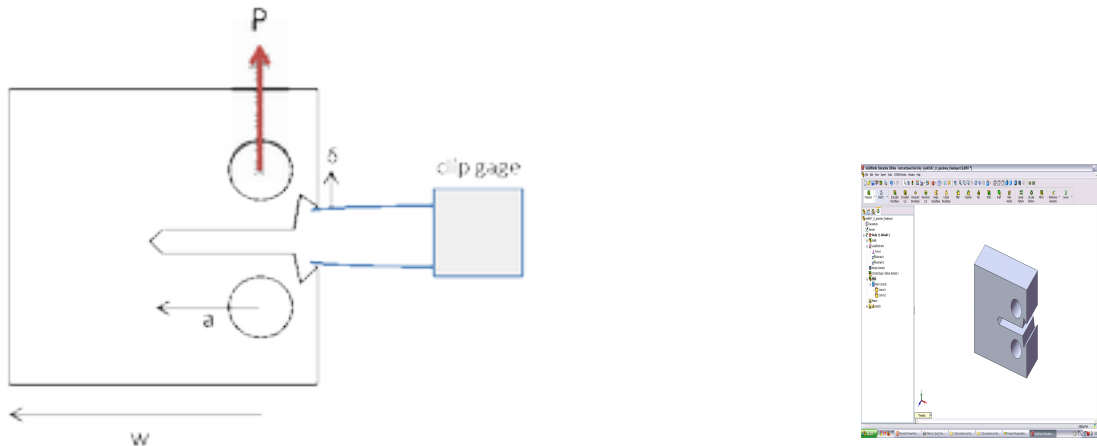

Figure 161618 - Model of compact tension specimen.

The snapshots were generated by measuring the deformations at the notch opening of the C(T) specimen as to replicate a standard fracture experiment with a clip gage. Various crack length sizes were then implemented via FEM that ranged from 0.35 - 0.55 in. to create the snapshot

matrix **U**, with a total of 21 snapshots *M*. Next, the eigenvalues of the covariance matrix **C** were calculated and truncated after the 5th eigenvalue of a possible 21, as shown in Table 10Table 10Table 10. In this example, the inverse crime was avoided by calculating the initial snapshot deformations using linear elements within the FEM software. Likewise, the experimental measurements were estimated using parabolic tetrahedral elements for higher experimental accuracy; this will also allow for a more conservative estimate of the crack length.

Table 10 - Table of truncated eigenvalues of fracture mechanics application

	λ_1	λ_2	λ_3	λ_4	λ_5
λ	2.17E+08	1.81E+01	3.23E+00	3.21E+00	1.25E+00

The experimental data was then obtained by adding a noise of ± 10 % of the mean value to the FEM solution. A plot of the deformation and error can be seen in Figure 17Figure 17Figure 19 and Table 11Table 11Table 11.
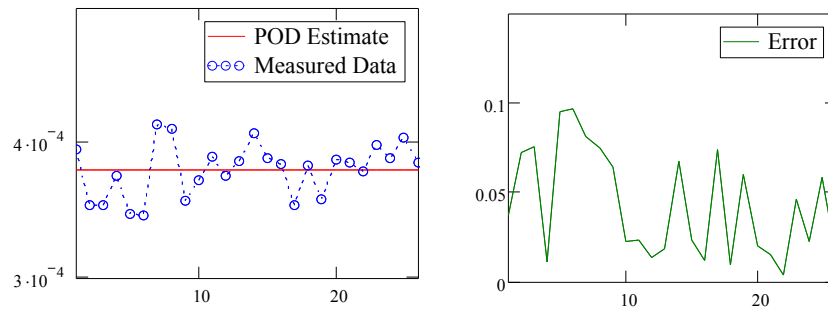
Figure 171719 - Deformation (left) and error (right) for ± 10% noise solution under Mode 1 loading.

Table 11 - Table of POD-RBF estimated crack lengths at various amounts of added noise

	Actual (in.)	No Noise	± 5 % Noise	± 10 % Noise
Crack Length	0.416	0.43749	0.43760	0.43766

By observing the deformations, it is easy to see the least squares fit goes provides a good estimate of the mean of data, despite the noisy solutions. This allows the POD-RBF inverse routine to optimally estimate the crack length with minimal error in regard to the initial snapshot matrix developed.

4. Conclusions

The POD-RBF inverse technique is successfully applied to the parameter estimation problem in a variety of examples. The numerical investigations provided herein illustrate that the POD based inverse technique is robust to measurement errors, even in the presence of relatively large error. Moreover, the POD-RBF inverse approach provides an efficient means of reducing the size and degrees of freedom of the problem while also optimizing accuracy of the solution to be determined. With the addition of a regularization parameter presented inside the least squares

objective function(s), the solution converges quickly. We also show that POD basis can be indentified with some of the analytical eigenfunctions of a heat conduction problem in a square and with these same eigenfunctions in an L-shaped domain constructed from an imbedding square region. The POD-RBF inverse method described in this paper

provides a computationally efficient framework for nondestructive estimation a unknown system parameters.

5. References

[1]   Pearson K (1901) On lines planes of closes fit to system of points in space. The London, Edinburgh and Dublin Philosophical Magazine and Journal of Science, **2**, 559–572.

[2]   Karhunen K (1946) Ueber lineare Methoden der Wahrscheinigkeitsrechnung. *Ann Acad Sci Fennicae A1 Math., Phys.,* **37,** 3–79.

[3]   Loeve MM (1955) *Probability theory*. Van Nostrand, Princeton, NY.

[4]   Hotelling H (1983) Analysis of complex of statistical variables into principal components. *J Educ Psychol.,* **24**, 417–441

[5]   Sirovich, L. (1995). Empirical Eigenfunctions and Low Dimensional Systems. In: L. Sirovich, *New Perspective in Turbulence*. Springer-Verlag.

[6]   Feeney, B. F., & Kappangantu R. J., (1998) On the Physical Interpretation of Proper Orthogonal Modes in Vibrations. *Sound Vibrations,* **211**, 607-616.

[7]   Wu CG, Liang YC, Lin WZ, Lee HP, Lim SP (2003) A note on equivalence of proper orthogonal decomposition methods. *J Sound Vibration,* **265,** 1103–1110.

[8]   Press, W.H, Teukolsky, S.A., Vetterling, W.T., & Flannery, B.P. (1992). Numerical Recipes in FORTRAN 77. New York, NY: Cambridge University Press.

[9]   Tikhonov A.N., Arsenin V.A. (1994) Solution of ill-posed problems. John Willey and Sons, New York.

[10]   Alifanov, O.M., 1994, Inverse Heat Transfer Problems, Springer-Verlag, Berlin.

[11]   Beck J.V., Blackwell B., St. Clair C.R., (1985) Inverse heat conduction: Ill-posed problems. John Willey and Sons, New York.

[12]   Ozisik MN, Orlande HRB (2000) Inverse heat transfer: Fundamentals and applications. Taylor & Francis, New York

[13]   Bialecki, R.A., Kassab, A.J., & Fic, A. (2004). Proper orthogonal decomposition and modal analysis for acceleration of transient fem thermal analysis. *International Journal*

for Numerical Methods in Engineering, **62**,774-797.

[14]   Fic, A, Bialecki, R.A., and Kassab, A.J. (2005). Solving transient nonlinear heat conduction problems by proper orthogonal decomposition and the finite-element method. *Numerical Heat Transfer*, **48,** 103-124.

[15]   Ostrowski, Z, Bialecki, R.A., and Kassab, A.J. (2005). Estimation of constant thermal conductivity by use of proper orthogonal decomposition. *Computational Mechanics*, **37**, 52-59.

[16]   Ostrowski, Z., Białecki, R. A. and Kassab, A. J. (2008) 'Solving inverse heat conduction problems using trained POD-RBF network inverse method', Inverse Problems in Science and Engineering, **16**, (1), 39-54.

[17]   Klimanek, A. (2010). Numerical modeling of heat, mass and momentum transfer in natural draft wet cooling tower. *PhD thesis*, Gliwice: Silesian University of Technology, Poland.

[18]   Rogers, C. (2010). Parameter Estimation in Heat Transfer and Elasticity using trained POD-RBF network inverse methods. *M.Sc. thesis*: University of Central Florida, Orlando,
USA.

[19]   Ostrowski, Z, Klimanek, A, & Bialecki, R.A. (2010). CFD two-scale model of a wet natural draft cooling tower. Numerical Heat Transfer, **57**, 119-137.

[20]   Sanford, R.J. (2003). Principles of fracture mechanics. Upper Saddle River, NJ: Pearson Education, Inc.

[21]   Anderson, T.L. (2005). Fracture mechanics: fundamentals and applications. Boca Raton, FL: CRC Press.

[22]   Hardy, R.L., (1971) Multiquadric equations of topolography and other irregular surfaces. Journal of Geophysical Research, **76**, 1905–1915

[23]   Hardy, R.L., (1990) Theory and applications of the multiquadricbiharmonic method: 20 years of discovery 1968–1988. Computational Mathematics with Applications, **19**, (8–9):163–208

[24]   Cheng, A.H.-D., Golberg, M.A., Kansa, E.J., Zammito, G., (2003), Exponential Convergence and H-c Multiquadric Collocation Method for Partial Differential Equations. Numerical Methods in P.D.E.,**19**, (5), 571-594.

[25]   Divo, E.A. and Kassab, A.J., (2007), An Efficient Localized RBF Meshless Method for Fluid Flow and Conjugate Heat Transfer. ASME Journal of Heat Transfer, **129**, 124-136.

[26] Divo, E. and Kassab, A.J., (2008), Localized Meshless Modeling of Natural Convective Viscous Flows. Numerical Heat Transfer, Part B: fundamentals , **53**, 487–509.

[27] Divo, E. , Kassab, A.J., Kapat, J.S., and Chyu, M.K., (1999), Retrieval of Multidimensional Heat Transfer Coefficient Distributions Using an Inverse BEM-Based Regularized Algorithm: numerical and experimental results, ASME Paper HTD-Vol. 364-1, 235-244.

[28] Kassab, A.J., Divo, E., Kapat, J.S., and Chyu, M.K., (2005), Retrieval of Multi-Dimensional Heat Transfer Coefficient Distributions Using an Inverse-BEM-Based Regularized Algorithm: Numerical and Experimental Examples. Engineering Analysis, **29**, (2),150-160.

[29] Hansen, P.C., and O'Leary, D.P., (1993). The use of the L-curve in the regularization of discrete ill-posed problems. SIAM Journal of Scientific Computing, **14,** 1487-1503.

[30] Hansen, P.C., Jensen, T.K., and Rodriguez, G., (2007) An adaptive pruning algorithm for the discrete L-curve criterion. Journal of Computational and Applied Mathematics, **198**, 483-492.

[31] A. Wirgin, The inverse crime. Online publication available at: http://arxiv.org/pdf/math-ph/0401050v1.pdf

[32] Comino, L, & Gallego, R. (2005). Material constants identification in anisotropic materials using boundary element techniques. Inverse Problems in Science & Engineering, **13**, (6), 635-654.

[33] Znaidia, S, Mzali, F, Sassi, l, Mhimid, A, & Jemni, A. (2005). Inverse problem in a porous medium: estimation of effective thermal properties. Inverse Problems in Science & Engineering, **13**,(6), 581-594.